

Ultrafast Ferroelectric Ordering on the Surface of a Topological Semimetal MoTe_2

Yanan Dai,^{||} Qijing Zheng,^{||} Mark E. Ziffer, Daniel Rhodes, James Hone, Jin Zhao,^{*} and Xiaoyang Zhu^{*}

Cite This: *Nano Lett.* 2021, 21, 9903–9908

Read Online

ACCESS |

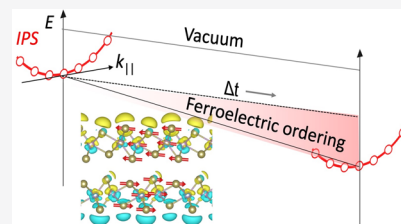
Metrics & More

Article Recommendations

Supporting Information

ABSTRACT: Transient tuning of material properties by light usually requires intense laser fields in the nonlinear excitation regime. Here, we report ultrafast ferroelectric ordering on the surface of a paraelectric topological semimetal $1\text{T}'\text{-MoTe}_2$ in the linear excitation regime, with the order parameter directly proportional to the excitation intensity. The ferroelectric ordering, driven by a transient electric field created by electrons trapped ångströms away from the surface in the image potential state (IPS), is evidenced in two-photon photoemission spectroscopy showing the energy relaxation rate proportional to IPS electron density, but with negligible change in the free-electron-like parallel dispersion. First-principles calculations reveal an improper ferroelectric ordering associated with an anharmonic interlayer shearing mode. Our findings demonstrate an ultrafast charge-based pathway for creating transient polarization orders.

KEYWORDS: ultrafast ferroelectricity, image potential states, 2D materials, TMD



Nonequilibrium states of matter offer unprecedented insights into structure–property relationships hidden from the ground state. Prominent examples include transient ferroelectricity,^{1–4} superconductivity,^{5,6} and charge density waves,⁷ all formed under intense laser fields. Here, we focus on transient ferroelectric polarization. Light-induced transient ferroelectric ordering has been demonstrated in bulk SrTiO_3 with terahertz or mid-IR pulse excitations, but only in the strongly nonlinear excitation region.^{1–4} In these examples, the intense laser fields are needed to transiently drive the transverse optical (TO) soft phonon mode with sufficient ionic displacements to the symmetry-breaking ferroelectric phase from the nominally inversion-symmetric phase.^{8,9} The advent of van der Waals layered ferroelectric semimetals^{10,11} opens up a new pathway for the creation and control of two-dimensional (2D) ferroelectricity, while spontaneous polarization usually vanishes for bulk semimetals or metals due to strong depolarization.¹² The unique 2D property in the distorted phases of transition metal dichalcogenides has been attributed to an improper ferroelectric mechanism,¹³ which is distinct from conventional soft-mode driven process. Instead of screening the electrical polarizations, itinerant electrons in these 2D semimetals give rise to uncompensated charge distributions associated with an interlayer shearing mode that drives the structural phase transition,¹⁴ leading to spontaneous surface-normal polarizations.

Transient changes of lattice symmetry in such atomically thin two-dimensional (2D) ferroelectric semimetals, and thus the suppression of ferroelectric polarizations, has been realized in $\text{T}_d\text{-WTe}_2$ and $\text{T}_d\text{-MoTe}_2$ on subpicosecond scales via the excitation of phase-determining interlayer shearing mode by intense visible to THz pulses.^{15–17} Ultrafast symmetry

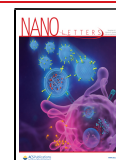
switching in centrosymmetric $1\text{T}'\text{-MoTe}_2$ has also been achieved via excitation of the interlayer shearing mode.¹⁸ Besides promising applications in ultrafast switching,^{19–21} the corresponding inversion symmetry breaking in these materials also splits their degenerate Dirac fermions into paired topologically protected Weyl fermions of opposite chirality.^{22–24} They are effectively separated monopoles of Berry curvatures that cause exotic physics such as axial magneto-electric coupling^{25,26} and chiral anomaly,²⁷ which can be precisely controlled via tuning of their lattice symmetry and thus the ferroelectric polarizations.¹⁵ Here, we report a new pathway to transient ferroelectric ordering of electric polarizations on the surface of the paraelectric semimetal $1\text{T}'\text{-MoTe}_2$ (Figure 1a, and see Supporting Information for detailed discussion of crystal phases) at room temperature: electrons trapped by the image potential create a surface-normal electric field on the femtosecond time scale and transiently induce mesoscopic sheet-like polarization, with the order parameter scaling linearly with laser field intensity.

Image potential states, Figure 1b, are a series of Rydberg states/resonances formed in the Coulomb potential between a transiently excited electron (blue sphere) on the surface of the material and its image charge (red sphere).^{28–30} The electron is confined by the IP in the surface normal direction, but it is

Received: August 1, 2021

Revised: November 11, 2021

Published: November 17, 2021



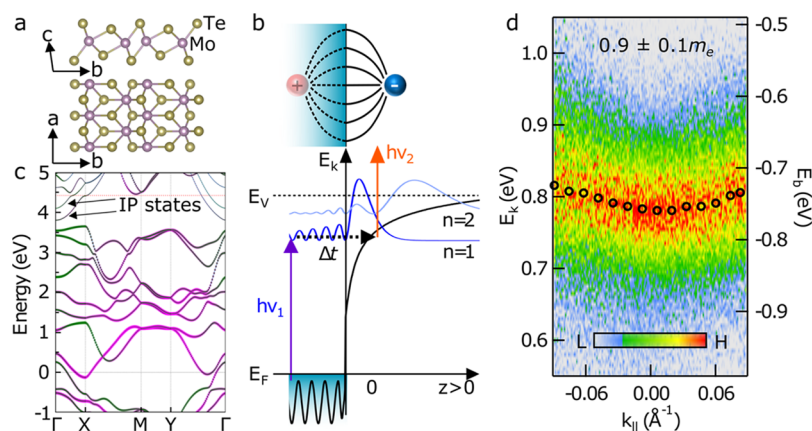


Figure 1. Image potential state on 1T'-MoTe₂. (a) Crystal structures of layered 1T'-MoTe₂ in the *a*-*c* and *a*-*b* plane; purple and green spheres are Mo and Te atoms, respectively. (b) Upper: Schematic of the IPS formation. An excited electron (blue sphere) is transiently trapped a few ångströms away from the material surface by the image potential as represented by a fictitious hole (red sphere). Lower: tr-2PPE experiment, where a UV pulse ($h\nu_1$) promotes an electron from the Fermi sea to the IPS (dark and light blue curves for $n = 1$ and 2 , respectively). The temporal dynamics is established by the probe pulse ($h\nu_2$) which ionizes the IPS electron detection with energy and parallel momentum resolution after a controlled time delay. (c) Calculated band structure (referenced to the Fermi level) of a MoTe₂ monolayer, with contributions from Mo and Te atoms denoted by green and purple colors. The lowest two IP states are indicated by the black arrows. (d) Pseudo-color plot of angle (parallel momentum, k_{\parallel}) resolved 2PPE spectra of the $n = 1$ IPS at $\Delta t = 0$ fs and $T = 294$ K, with pump and probe $h\nu = 4.59$ and 1.54 eV, respectively. The hollow circles mark the Lorentzian fitted IP peak positions, giving $m_{\text{eff}} = 0.9 \pm 0.1 m_e$, where m_e is the free electron mass. Color scale indicates photoelectron counts from low (L) to high (H).

free in the surface plane, giving rise to a series of free-electron-like parallel dispersions:^{29,31}

$$E_{n,k_{\parallel}} = E_n + \frac{\hbar^2 k_{\parallel}^2}{2m_{\text{eff}}} \quad (1)$$

$$E_n = E_{\text{vac}} - \beta^2 \frac{0.85(\text{eV})}{(n+a)^2} \quad (2)$$

where $n = 1, 2, \dots$ is the quantum number of the IPS, \hbar is the reduced Planck's constant, k_{\parallel} is the parallel momentum vector, and m_{eff} is the electron effective mass, usually the same as the free electron mass, m_e . $\beta = (\epsilon - 1)/(\epsilon + 1)$, where ϵ is the relative permittivity of the material; a is the so-called quantum defect and accounts for the coupling of the IPS to bulk states at the material/vacuum interface; and E_{vac} is the vacuum level. Using a reported $\epsilon \sim 19$ in the THz region³² and assuming $a = 0$, we estimate $E_1 \sim 0.69$ eV below E_{vac} in close agreement with the reported IPS energy on the surface of the semimetal bismuth.³¹ Density functional theory (DFT) calculation on monolayer MoTe₂ also revealed the presence of the IPS (arrows in Figure 1c) with free electron-like parallel dispersions. Because IPS electrons are transiently trapped in the vacuum, ångströms away from the material as seen in their probability densities $|\psi|^2$ in Figure 1b, they are sensitive probes of the surface dielectric environment, e.g., in the screening of an IPS electron by molecular adsorbates in solvation or polaron formation.^{33–36}

To probe the transient polarization ordering driven by the IPS electrons, we directly measure the lowest ($n = 1$) IPS using time-resolved two-photon photoemission (tr-2PPE) spectroscopy;³⁷ a UV pump pulse of $h\nu_1 = 4.59$ eV with pulse duration < 100 fs (Figure 1b and Figure S1) excites an electron from the Fermi level of an *in situ* cleaved 1T'-MoTe₂ to its $n = 1$ IPS, with a near-IR probe pulse (< 50 fs) of $h\nu_2 = 1.54$ eV ionizing the IPS electron at a precisely controlled time delay (Δt) for spectroscopic detection with angular (k_{\parallel}) resolution (see the Supporting Information for experimental details). Figure 1d

plots the room temperature ($T = 294$ K) angle-resolved 2PPE spectra at $\Delta t = 0$ fs. At $k_{\parallel} = 0$, the electron kinetic energy $E_k = 0.79 \pm 0.01$ eV corresponds to a binding energy of $E_b = 0.75 \pm 0.01$ eV, which is close to the estimated value of 0.69 eV. The free-electron-like dispersion is marked by the hollow-circles (center-of-mass), which gives $m_{\text{eff}} = 0.9 \pm 0.1 m_e$ by a quadratic fitting.

The IPS relaxes in energy with increasing Δt , as shown by the k_{\parallel} -integrated tr-2PPE spectra in Figure 2a. The peak energy (white circles) relaxes by $\Delta E \sim -50$ meV for $\Delta t \sim 200$ fs, after which there is negligible signal, likely due to efficient scattering into near resonant conduction bands (see DFT band structure in Figure 1c). Since 1T'-MoTe₂ is a semimetal, not a semiconductor, the energy relaxation mechanism specific for a semiconductor due to the surface photovoltage effect^{38,39} cannot be responsible here. Also, the excitation laser pulse energy used here is over 2 orders of magnitude lower that required for the observation of space charge effect as reported for photoemission from metal surfaces.⁴⁰ The observed ~ 100 fs time scale for energy relaxation is characteristic of phonon responses.

In conventional centrosymmetric semimetals, such as graphene, no energy relaxation of the IP electron has been reported,⁴¹ because there lacks an efficient phonon or phonon-induced charge response in screening the IP electron on the ~ 100 fs scale. Instead, the IP energy is dominantly determined by the electronic polarization nearly instantaneously (< 10 fs).⁴² In the case of strongly polarizable molecular adsorbates, polar molecular dipoles can screen an IP electron via local reordering to form a small polaron, as reflected in the time-dependent decreases in IP electron energy and disappearance of dispersion.^{33–36} In stark contrast to these previous reports where image electron energy relaxation is always accompanied by wave function localization (m_{eff} increases on femtosecond time scales),^{33–36} no change in m_{eff} is observed with time in the present case. This is evidenced by the rigid downward shift of the free-electron-like dispersion from $\Delta t = 50$ fs (Figure 2b)

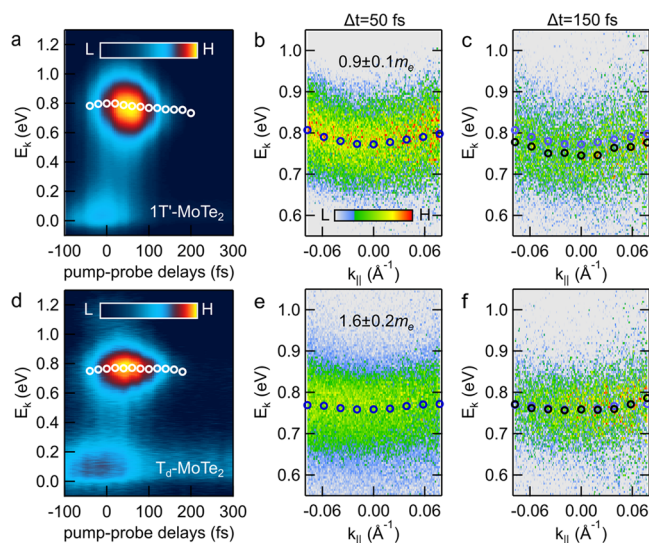


Figure 2. Relaxation of IPS electron on 1T'- and T_d-MoTe₂. (a) Pseudocolor plots of $k_{||}$ -integrated tr-2PPE spectra as a function of pump–probe delays (Δt), taken at a sample temperature of $T = 294$ K. White circles indicate the IP state peak positions obtained by Lorentzian fitting. (b, c) Angle resolved 2PPE spectra showing the free electron like dispersion of the IPS at $\Delta t = 50$ fs (b) and 150 fs (c). IPS peaks positions are marked by blue circles in part b (reproduced in part c), and black circles in part c. (d–f) IPS electron relaxation dynamics on T_d-MoTe₂ at 116 K. (d) $k_{||}$ -integrated tr-2PPE spectra as a function of pump–probe delay; (e, f) parallel dispersions of the IPS at $\Delta t = 50$ and 150 fs, respectively. IPS peaks positions are marked by blue circles in part e (reproduced in part f), and black circles in part f. In both parts a and d, photoelectron signal near zero kinetic energy is assigned to secondary electrons (for $\Delta t \geq 0$ fs) and hot electrons photoexcited by the near-IR pulse and probed by the UV pulse (for $\Delta t \leq 0$ fs).

to $\Delta t = 150$ fs (Figure 2c). Therefore, instead of localized screening as in solvation or polaron formation,^{33–36} the polarization field which screens the IPS electrons on the paraelectric 1T'-MoTe₂ surface is in the surface normal direction only and not in the 2D surface plane. Thus, we call this kind of collective and 2D sheet-like dielectric response *ferroelectric ordering*, where the polarization order originates from the directional redistribution of fluctuating charge distributions associated with an anharmonic phonon mode, as detailed in DFT calculations below. We note that, unlike conventional ferroelectricity which reverses under certain coercive field, the occupation of the IPS creates a transient normal electric field only in one direction, and the symmetry of 1T'-MoTe₂ dictates that the ferroelectric ordering on the surface should be reversible if the IP electric field is reversed, as we show below in DFT calculations, although the electric field from the IP electrons cannot be reversed experimentally.⁴³ The ferroelectric ordering on the surface of 1T'-MoTe₂ by IPS electrons resembles the ferroelectric polarons proposed for charge carrier screening in lead halide perovskites.^{44,45}

Consistent with the interpretation of transient ferroelectric ordering on the paraelectric 1T'-MoTe₂ surface, we show negligible screening in response to IPS occupation on the surface of the ferroelectric T_d-MoTe₂ at $T = 116$ K; the structural phase transition from 1T' to T_d phase occurs at ~ 250 K.⁴⁶ There is no measurable energy relaxation of the IPS within its lifetime, Figure 2d, and the dispersions at $\Delta t = 50$ fs (Figure 2e) and 150 fs (Figure 2f) are superimposable.

Because ferroelectric polarizations are well established at 116 K, only an electric field that is on the order of its coercive field can switch or realign the polarization domains. Therefore, we conclude that the electric field from the transient IPS electrons is insufficient to change the intrinsic ferroelectric order originating from spontaneous symmetry breaking, thus giving negligible change in the IP dynamics. Interestingly, however, the IPS on the T_d-MoTe₂ surface shows measurably higher effective mass, $m_{\text{eff}} \sim 1.6 \pm 0.2 m_e$, which we attribute to deviation from the free electron landscape in the surface plane due to existing domains of opposite polarizations⁴⁶ that induce lateral confinement to the IPS wave function.⁴⁷

Strong evidence for the collective screening of IPS electrons in 1T'-MoTe₂ comes from the pump pulse fluence (ρ) dependence. Within the pump fluences ($\rho < 3 \mu\text{J}/\text{cm}^2$) used the 2PPE intensity scales linearly with ρ , Figure 3a, establishing

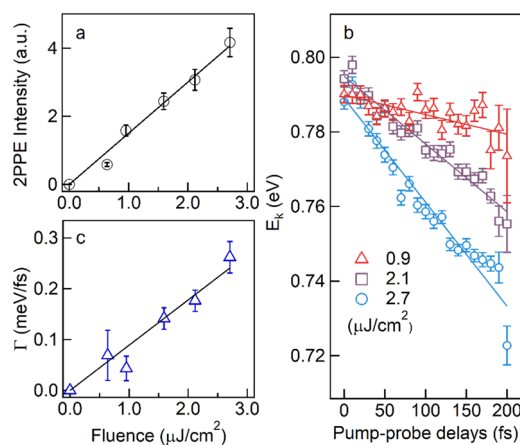


Figure 3. Fluence-dependent IP state dynamics. (a) 2PPE intensity as a function of pump fluence (open circles) at room temperature. The solid line is a linear fit. (b) IPS energy as a function of pump–probe delay for three selected excitation fluences (0.9, 2.1, 2.7 $\mu\text{J}/\text{cm}^2$). The solid lines are linear fits to the data. (c) IPS energy relaxation rate (Γ) as a function of laser pump fluence. The solid line is a linear fit.

the single particle nature of excitation. In this linear and low excitation region, the energy relaxation dynamics of each excited single particle should be independent of ρ , as is the case in all previous reports on IPS electron energy relaxation due to polaron formation or solvation.^{33–36} In contrast, we find that the IPS electron energy relaxation rate strongly depends on the pump fluence, as shown by the extracted IPS peak positions at selected excitation densities in Figure 3b. The energy relaxation rate (Γ), obtained from linear fits to the data in Figure 3b, depends linearly on ρ , Figure 3c. This result supports the collective nature of the screening mechanism, i.e., transient ferroelectric ordering. The order parameter is given by the collective polarization, P , which is directly proportional to the transient electric field, E_{IPS} , in the linear response region. Moreover, E_{IPS} determined from the population of the IPS, linearly scales with the electron excitation density in a simple capacitor model. The magnitude of the transient polarization orders can be directly tuned via photoexcitation densities. The maximum effective electric field associated with the IP electron is estimated to be $E_{\text{eff}} \sim 7 \text{ mV}\cdot\text{\AA}^{-1}$ based on a capacitor model (Supporting Information),⁴⁸ with the excitation density of $\sim 3.6 \times 10^{11} \text{ cm}^{-2}$ at an UV pump pulse fluence of 2.7 $\mu\text{J}/\text{cm}^2$ used in Figure 2a–c. Note that the field estimated from IP

polarization is of the same order as the spontaneous polarization density of T_d -MoTe₂.³⁹

To understand how transiently induced ferroelectric ordering collectively screens electrons in the IPS, we carry out DFT calculations for $1T'$ -MoTe₂ subjected to an effective surface-normal electric field E_{eff} associated with the population of IPS (see Supporting Information for details). We plot in Figure 4a

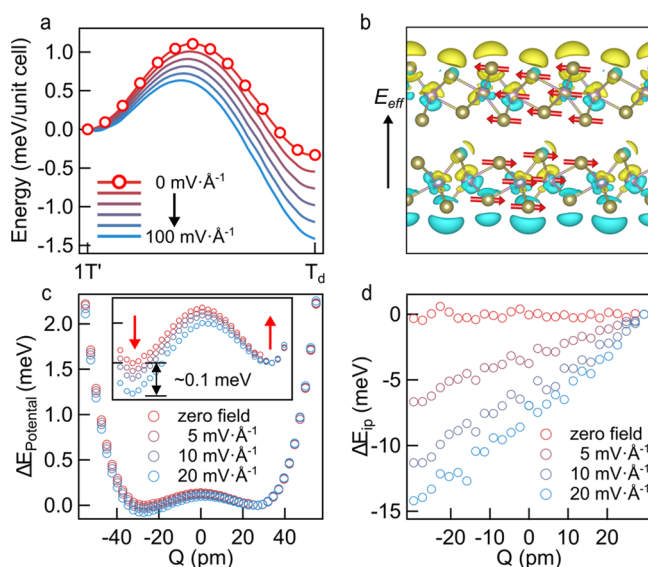


Figure 4. Calculated polarization response of $1T'$ -MoTe₂ to transient electric field from IPS electrons. (A) Total energy per unit cell along the bulk $1T'$ to T_d -phase transition in the presence of an effective normal electric field (0 – 100 $\text{mV}\cdot\text{\AA}^{-1}$). (B) Net differential charge distribution (yellow, positive; blue, negative) due to the interlayer shearing mode, showing the charge redistribution when the system is subjected to $E_{eff} = 20$ $\text{mV}\cdot\text{\AA}^{-1}$ from that at zero field. The red arrows on the lattice indicate the interlayer shearing mode. (C) Free energy surfaces associated with the anharmonic A_g mode in bilayer MoTe₂, in the presence of increasing effective electric field. The inset shows the enlarged view of the flat bottom, and the magnitude of the energy surface the tilting. (D) Relaxation of IPS energy with respect to E_F for selected $E_{eff} = 0$ – 20 $\text{mV}\cdot\text{\AA}^{-1}$.

the total energy per unit cell along the paraelectric ($1T'$) to ferroelectric (T_d) phase transition pathway for MoTe₂ for selected E_{eff} . Increasing E_{eff} favors the downward-polarized T_d over the $1T'$ phase, suggesting that the IP electron can preferably modify the materials potential energy. Without loss of generality, we model the lattice screening of IPS electrons, i.e., E_{eff} by the induced polarizations in the thinnest MoTe₂ structure possessing surface normal polarizations, i.e., a bilayer (see Supporting Information for details); a similar collective response is expected for thicker crystals. We focus on analyzing the responses of the anharmonic phonon modes to the presence of E_{eff} because harmonic phonon modes respond little to applied E_{eff} . Among the modes contributing to the polarization response in screening the field, we find that the mode at 11 cm^{-1} plays dominant role in IPS energy relaxation (Figure S3d). This mode corresponds to the interlayer shear motion along the b -axis (arrows in Figure 4b) and is known to govern the surface normal polarizations and the ferroelectric phase transition in bulk crystals.^{14–16} In the employed bilayer model, however, such a shearing mode only affects the magnitude of the pre-existing surface-normal polarization without leading to a phase transition into T_d phase.

The calculated potential energy surface along this shear mode coordinate (Q), Figure 4c, reveals the double well character representing up and down surface polarizations, and this double well is tilted to the polarized configuration in response to the normal electric field up to a nearly saturation field of ~ 20 $\text{mV}\cdot\text{\AA}^{-1}$. However, the magnitude of the energy stabilization (Figure 4c inset) is $\sim 10^2$ smaller than the experimentally observed energy relaxation of the IPS. This is understood from the semimetallic MoTe₂ being an improper ferroelectric^{13,14,49} and the electron density redistribution associated with displacement in Q of the shear mode is expected to dominate the polarization response. This is confirmed in Figure 4b, which shows the differential charge distribution solely resulting from lattice distortion for the preferred downward polarization, before and after the application of $E_{eff} = 20$ $\text{mV}\cdot\text{\AA}^{-1}$. The interlayer shearing mode thus induces an out-of-plane charge redistribution, with positive (green) charge concentrating on the top surface where IPS electrons reside and negative charge (blue) on the bottom surface. Note that an effective IP field-reversal can be considered by analyzing the redistributed charge from the bottom layer, thus giving rise to an opposite polarization compared to the top layer. The induced polarization occurs faster than the associated vibrational period as E_{eff} may stabilize pre-existing charge fluctuations and the collective motion involved is only a fraction of the vibrational period. Therefore, despite the pure ionic displacement due to the shear mode contributing negligibly to screening the IPS, the associated charge redistribution, which determines the improper ferroelectricity in MoTe₂, amplifies the screening effect by $\sim 10^2$, shifting the IP state energy by ~ 15 meV (Figure 4d), as well as the local vacuum level,³³ schematically shown in Figure S4. Such large electronic polarization associated with a small lattice, unlike conventional displacive ferroelectrics described in Landau theory,⁵⁰ is unique to the MoTe₂/WTe₂ systems. This collective screening response to the presence of an external electric field is nearly identical with the improper ferroelectric mechanism in MoTe₂,^{13,14,49} and thus we call this response ferroelectric ordering. Charge-induced lattice motion in the bulk initiates the anharmonic low frequency shearing mode as observed in transient reflectivity changes.¹⁸ Our experiment determines the transient surface ferroelectric polarization, which may be attributed to the response of this phonon mode to transient electric field.

We note that the calculated IP energy relaxation due to the shear mode is smaller than that observed in tr-2PPE experiments. This can be understood by two factors: (1) There is an underestimation of the energy barrier and polarization energy of ferroelectric MoTe₂ by the approximations in DFT calculations which may lead to underestimation of the magnitude of the screening field.^{15,49} (2) A number of other anharmonic phonon modes also respond to E_{eff} and contribute to the total polarization response. Note that the calculation above explores the electric field in one direction, and the symmetry of the system dictates that the polarization response is reversed when the applied electric field is reversed.

The findings presented above demonstrate a new pathway for transient ferroelectric ordering of sheet-like surface polarization fields by IPS electrons on 10^2 fs time scale and with the order parameter (polarization) scaling linearly with pump pulse fluence. Moreover, such ferroelectric ordering is a

direct consequence of a novel form of dielectric screening, with its geometry resembling ferroelectric large polaron screening^{44,45} proposed to account for the remarkable charge carrier screening and optoelectronic properties of lead halide perovskites. Finally, because the electronic band structure topology of MoTe₂ at the Fermi level is sensitive to the material inversion symmetry, the effective surface electric field of IPS electrons, which can transiently modify the local lattice and electronic polarizations, may serve to control the nontrivial electronic band topology, such as Lifshitz transition,⁵¹ Weyl point separation,^{15,52} and magnetoelectric gyrotropic response,⁵³ as well as inducing magnetic monopoles and fractional anion excitations for quantum computations²⁵ via coupling to axial current between Weyl nodes²⁶ on ultrafast time scales.

■ ASSOCIATED CONTENT

SI Supporting Information

The Supporting Information is available free of charge at <https://pubs.acs.org/doi/10.1021/acs.nanolett.1c02965>.

Details of (1) the MoTe₂ sample synthesis and preparation, (2) the time-resolved two-photon photoemission spectroscopy setup, (3) analysis of the transient field strength associated with the image potential state, and (4) the numerical setups of the DFT calculation and the corresponding analysis of the bulk transition energy barrier and other anharmonic phonon modes that are potentially involved in the ferroelectric screening (PDF)

■ AUTHOR INFORMATION

Corresponding Authors

Xiaoyang Zhu – Department of Chemistry, Columbia University, New York, New York 10027, United States; orcid.org/0000-0002-2090-8484; Email: xyzhu@columbia.edu

Jin Zhao – Department of Physics, University of Science and Technology of China, Hefei, Anhui 230026, China; Email: zhaojin@ustc.edu.cn

Authors

Yanan Dai – Department of Chemistry, Columbia University, New York, New York 10027, United States

Qijing Zheng – Department of Physics, University of Science and Technology of China, Hefei, Anhui 230026, China; orcid.org/0000-0003-0022-3442

Mark E. Ziffer – Department of Chemistry, Columbia University, New York, New York 10027, United States; orcid.org/0000-0003-2324-3876

Daniel Rhodes – Department of Mechanical Engineering, Columbia University, New York, New York 10027, United States; orcid.org/0000-0002-7651-3211

James Hone – Department of Mechanical Engineering, Columbia University, New York, New York 10027, United States

Complete contact information is available at: <https://pubs.acs.org/doi/10.1021/acs.nanolett.1c02965>

Author Contributions

[†]Y.D. and Q.Z. contributed equally.

Notes

The authors declare no competing financial interest.

■ ACKNOWLEDGMENTS

X.Z. acknowledges the Vannevar Bush Faculty Fellowship through the Office of Naval Research Grant # N00014-18-1-2080 for supporting the tr-2PPE experiment and the US Department of Energy, Office of Energy Science, Grant DE-SC0010692, for supporting sample preparation and characterization. J.Z. acknowledges National Natural Science Foundation of China (NSFC), Grant No. 11620101003, 11974322. M.E.Z. acknowledges postdoctoral fellowship support by the U.S. Department of Energy Office of Energy Efficiency and Renewable Energy administered by the Oak Ridge Institute for Science and Education (ORISE) for the DOE. ORISE is managed by Oak Ridge Associated Universities (ORAU) under DOE Contract Number DE-SC0014664. All opinions expressed in this paper are the author's and do not necessarily reflect the policies and views of DOE, ORAU, or ORISE.

■ REFERENCES

- (1) Li, X.; Qiu, T.; Zhang, J.; Baldini, E.; Lu, J.; Rappe, A. M.; Nelson, K. A. Terahertz Field – Induced Ferroelectricity in Quantum Paraelectric SrTiO₃. *Science* **2019**, *364* (6445), 1079–1082.
- (2) Nova, T. F.; Disa, A. S.; Fechner, M.; Cavalleri, A. Metastable Ferroelectricity in Optically Strained SrTiO₃. *Science* **2019**, *364* (6445), 1075–1079.
- (3) Subedi, A. Proposal for Ultrafast Switching of Ferroelectrics Using Midinfrared Pulses. *Phys. Rev. B: Condens. Matter Mater. Phys.* **2015**, *92* (21), 214303.
- (4) Mankowsky, R.; von Hoegen, A.; Först, M.; Cavalleri, A. Ultrafast Reversal of the Ferroelectric Polarization. *Phys. Rev. Lett.* **2017**, *118* (19), 197601.
- (5) Fausti, D.; Tobey, R. I.; Dean, N.; Kaiser, S.; Dienst, A.; Hoffmann, M. C.; Pyon, S.; Takayama, T.; Takagi, H.; Cavalleri, A. Light-Induced Superconductivity in a Stripe-Ordered Cuprate. *Science* **2011**, *331* (6014), 189–191.
- (6) Kennes, D. M.; Wilner, E. Y.; Reichman, D. R.; Millis, A. J. Transient Superconductivity from Electronic Squeezing of Optically Pumped Phonons. *Nat. Phys.* **2017**, *13* (5), 479–483.
- (7) Kogar, A.; Zong, A.; Dolgirev, P. E.; Shen, X.; Straquadine, J.; Bie, Y.-Q.; Wang, X.; Rohwer, T.; Tung, I.-C.; Yang, Y.; et al. Light-Induced Charge Density Wave in LaTe₃. *Nat. Phys.* **2020**, *16* (2), 159–163.
- (8) Scott, J. F. Soft-Mode Spectroscopy: Experimental Studies of Structural Phase Transitions. *Rev. Mod. Phys.* **1974**, *46* (1), 83.
- (9) Lines, M. E.; Glass, A. M. *Principles and Applications of Ferroelectrics and Related Materials*; Oxford University Press: Oxford, U.K., 2001.
- (10) Fei, Z.; Zhao, W.; Palomaki, T. A.; Sun, B.; Miller, M. K.; Zhao, Z.; Yan, J.; Xu, X.; Cobden, D. H. Ferroelectric Switching of a Two-Dimensional Metal. *Nature* **2018**, *560* (7718), 336–339.
- (11) Yuan, S.; Luo, X.; Chan, H. L.; Xiao, C.; Dai, Y.; Xie, M.; Hao, J. Room-Temperature Ferroelectricity in MoTe₂ down to the Atomic Monolayer Limit. *Nat. Commun.* **2019**, *10* (1), 1–6.
- (12) Wurfel, P.; Batra, I. P. Depolarization-Field-Induced Instability in Thin Ferroelectric Films—Experiment and Theory. *Phys. Rev. B* **1973**, *8* (11), 5126.
- (13) Shirodkar, S. N.; Waghmare, U. V. Emergence of Ferroelectricity at a Metal-Semiconductor Transition in a 1T Monolayer of MoS₂. *Phys. Rev. Lett.* **2014**, *112* (15), 157601.
- (14) Yang, Q.; Wu, M.; Li, J. Origin of Two-Dimensional Vertical Ferroelectricity in WTe₂ Bilayer and Multilayer. *J. Phys. Chem. Lett.* **2018**, *9* (24), 7160–7164.
- (15) Sie, E. J.; Nyby, C. M.; Pemmaraju, C. D.; Park, S. J.; Shen, X.; Yang, J.; Hoffmann, M. C.; Ofori-Okai, B. K.; Li, R.; Reid, A. H.; et al. An Ultrafast Symmetry Switch in a Weyl Semimetal. *Nature* **2019**, *565* (7737), 61–66.
- (16) Zhang, M. Y.; Wang, Z. X.; Li, Y. N.; Shi, L. Y.; Wu, D.; Lin, T.; Zhang, S. J.; Liu, Y. Q.; Liu, Q. M.; Wang, J.; et al. Light-Induced

Subpicosecond Lattice Symmetry Switch in MoTe_2 . *Phys. Rev. X* **2019**, *9* (2), 21036.

(17) Ji, S.; Grånäs, O.; Weissenrieder, J. Manipulation of Stacking Order in $\text{T}_d\text{-WTe}_2$ by Ultrafast Optical Excitation. *ACS Nano* **2021**, *15* (5), 8826–8835.

(18) Fukuda, T.; Makino, K.; Saito, Y.; Fons, P.; Kolobov, A. V.; Ueno, K.; Hase, M. Ultrafast Dynamics of the Low Frequency Shear Phonon in $1\text{T}'\text{-MoTe}_2$. *Appl. Phys. Lett.* **2020**, *116* (9), 093103.

(19) Wang, Z.; Wu, H.; Burr, G. W.; Hwang, C. S.; Wang, K. L.; Xia, Q.; Yang, J. J. Resistive Switching Materials for Information Processing. *Nat. Rev. Mater.* **2020**, *5* (3), 173–195.

(20) Guo, J.; Chen, W.; Chen, H.; Zhao, Y.; Dong, F.; Liu, W.; Zhang, Y. Recent Progress in Optical Control of Ferroelectric Polarization. *Adv. Opt. Mater.* **2021**, 2002146.

(21) Chu, J.; Wang, Y.; Wang, X.; Hu, K.; Rao, G.; Gong, C.; Wu, C.; Hong, H.; Wang, X.; Liu, K.; et al. 2D Polarized Materials: Ferromagnetic, Ferrovalley, Ferroelectric Materials, and Related Heterostructures. *Adv. Mater.* **2021**, *33* (5), 2004469.

(22) Li, P.; Wen, Y.; He, X.; Zhang, Q.; Xia, C.; Yu, Z.-M.; Yang, S. A.; Zhu, Z.; Alshareef, H. N.; Zhang, X.-X. Evidence for Topological Type-II Weyl Semimetal WTe_2 . *Nat. Commun.* **2017**, *8* (1), 1–8.

(23) Deng, K.; Wan, G.; Deng, P.; Zhang, K.; Ding, S.; Wang, E.; Yan, M.; Huang, H.; Zhang, H.; Xu, Z.; et al. Experimental Observation of Topological Fermi Arcs in Type-II Weyl Semimetal MoTe_2 . *Nat. Phys.* **2016**, *12* (12), 1105–1110.

(24) Jiang, J.; Liu, Z. K.; Sun, Y.; Yang, H. F.; Rajamathi, C. R.; Qi, Y. P.; Yang, L. X.; Chen, C.; Peng, H.; Hwang, C. C.; et al. Signature of Type-II Weyl Semimetal Phase in MoTe_2 . *Nat. Commun.* **2017**, *8* (1), 1–6.

(25) Qi, X.-L.; Li, R.; Zang, J.; Zhang, S.-C. Inducing a Magnetic Monopole with Topological Surface States. *Science* **2009**, *323* (5918), 1184–1187.

(26) Nenzo, D. M.; Garcia, C. A. C.; Gooth, J.; Felser, C.; Narang, P. Axion Physics in Condensed-Matter Systems. *Nat. Rev. Phys.* **2020**, *2* (12), 682–696.

(27) Armitage, N. P.; Mele, E. J.; Vishwanath, A. Weyl and Dirac Semimetals in Three-Dimensional Solids. *Rev. Mod. Phys.* **2018**, *90* (1), 15001.

(28) Höfer, U.; Shumay, I. L.; Reuß, C.; Thomann, U.; Wallauer, W.; Fauster, T. Time-Resolved Coherent Photoelectron Spectroscopy of Quantized Electronic States on Metal Surfaces. *Science* **1997**, *277* (5331), 1480–1482.

(29) Chulkov, E. V.; Silkin, V. M.; Echenique, P. M. Image Potential States on Metal Surfaces: Binding Energies and Wave Functions. *Surf. Sci.* **1999**, *437* (3), 330–352.

(30) Silkin, V. M.; Zhao, J.; Guinea, F.; Chulkov, E. V.; Echenique, P. M.; Petek, H. Image Potential States in Graphene. *Phys. Rev. B: Condens. Matter Mater. Phys.* **2009**, *80* (12), 121408.

(31) Muntwiler, M.; Zhu, X. Y. Image-Potential States on the Metallic (111) Surface of Bismuth. *New J. Phys.* **2008**, *10* (11), 113018.

(32) Lezama, I. G.; Ubaldini, A.; Longobardi, M.; Giannini, E.; Renner, C.; Kuzmenko, A. B.; Morpurgo, A. F. Surface Transport and Band Gap Structure of Exfoliated 2H-MoTe_2 Crystals. *2D Mater.* **2014**, *1* (2), 021002.

(33) Miller, A. D.; Bezel, I.; Gaffney, K. J.; Garrett-Roe, S.; Liu, S. H.; Szymanski, P.; Harris, C. B. Electron Solvation in Two Dimensions. *Science* **2002**, *297* (5584), 1163–1166.

(34) Ge, N.-H.; Wong, C. M.; Lingle, R. L.; McNeill, J. D.; Gaffney, K. J.; Harris, C. B. Femtosecond Dynamics of Electron Localization at Interfaces. *Science* **1998**, *279* (5348), 202–205.

(35) Muntwiler, M.; Zhu, X.-Y. Formation of Two-Dimensional Polarons That Are Absent in Three-Dimensional Crystals. *Phys. Rev. Lett.* **2007**, *98* (24), 246801.

(36) Bovensiepen, U.; Gahl, C.; Stahler, J.; Bockstedte, M.; Meyer, M.; Balletto, F.; Scandolo, S.; Zhu, X.-Y.; Rubio, A.; Wolf, M. A Dynamic Landscape from Femtoseconds to Minutes for Excess Electrons at Ice-Metal Interfaces. *J. Phys. Chem. C* **2009**, *113* (3), 979–988.

(37) Giesen, K.; Hage, F.; Himpfel, F. J.; Riess, H. J.; Steinmann, W. Two-Photon Photoemission via Image-Potential States. *Phys. Rev. Lett.* **1985**, *55* (3), 300.

(38) Ogawa, M.; Yamamoto, S.; Fujikawa, K.; Hobara, R.; Yukawa, R.; Yamamoto, S.; Kitagawa, S.; Pierucci, D.; Silly, M. G.; Lin, C.-H.; et al. Relaxations of the Surface Photovoltage Effect on the Atomically Controlled Semiconductor Surfaces Studied by Time-Resolved Photoemission Spectroscopy. *Phys. Rev. B: Condens. Matter Mater. Phys.* **2013**, *88* (16), 165313.

(39) Yang, S.-L.; Sobota, J. A.; Kirchmann, P. S.; Shen, Z.-X. Electron Propagation from a Photo-Excited Surface: Implications for Time-Resolved Photoemission. *Appl. Phys. A: Mater. Sci. Process.* **2014**, *116* (1), 85–90.

(40) Passlack, S.; Mathias, S.; Andreyev, O.; Mittnacht, D.; Aeschlimann, M.; Bauer, M. Space Charge Effects in Photoemission with a Low Repetition, High Intensity Femtosecond Laser Source. *J. Appl. Phys.* **2006**, *100* (2), 024912.

(41) Nobis, D.; Potenz, M.; Niesner, D.; Fauster, T. Image-Potential States of Graphene on Noble-Metal Surfaces. *Phys. Rev. B: Condens. Matter Mater. Phys.* **2013**, *88* (19), 195435.

(42) Fauster, T.; Steinmann, W. Two-Photon Photoemission Spectroscopy of Image States. *Electromagn. Waves Recent Dev. Res.* **1995**, *2*, 347–411.

(43) Zhu, X.; Monahan, N. R.; Gong, Z.; Zhu, H.; Williams, K. W.; Nelson, C. A. Charge Transfer Excitons at van Der Waals Interfaces. *J. Am. Chem. Soc.* **2015**, *137* (26), 8313–8320.

(44) Miyata, K.; Zhu, X.-Y. Ferroelectric Large Polarons. *Nat. Mater.* **2018**, *17* (5), 379–381.

(45) Wang, F.; Fu, Y.; Ziffer, M. E.; Dai, Y.; Maehrlin, S. F.; Zhu, X.-Y. Solvated Electrons in Solids—Ferroelectric Large Polarons in Lead Halide Perovskites. *J. Am. Chem. Soc.* **2021**, *143* (1), 5–16.

(46) Huang, F.-T.; Joon Lim, S.; Singh, S.; Kim, J.-W. J.; Zhang, L.; Kim, J.-W. J.; Chu, M.-W.; Rabe, K. M.; Vanderbilt, D.; Cheong, S.-W. Polar and Phase Domain Walls with Conducting Interfacial States in a Weyl Semimetal MoTe_2 . *Nat. Commun.* **2019**, *10* (1), 1–9.

(47) Dutton, G.; Pu, J.; Truhlar, D. G.; Zhu, X.-Y. Lateral Confinement of Image Electron Wave Function by an Interfacial Dipole Lattice. *J. Chem. Phys.* **2003**, *118* (10), 4337–4340.

(48) Wang, J.; Ardelean, J.; Bai, Y.; Steinhoff, A.; Florian, M.; Jahnke, F.; Xu, X.; Kira, M.; Hone, J.; Zhu, X.-Y. Optical Generation of High Carrier Densities in 2D Semiconductor Heterobilayers. *Sci. Adv.* **2019**, *5* (9), No. eaax0145.

(49) Kim, H.-J.; Kang, S.-H.; Hamada, I.; Son, Y.-W. Origins of the Structural Phase Transitions in MoTe_2 and WTe_2 . *Phys. Rev. B: Condens. Matter Mater. Phys.* **2017**, *95* (18), 180101.

(50) Landau, L. D.; Lifshitz, E. M. *Course of Theoretical Physics*; Elsevier: Amsterdam, The Netherlands, 2013.

(51) Beaulieu, S.; Dong, S.; Tancogne-Dejean, N.; Dendzik, M.; Pincelli, T.; Maklar, J.; Xian, R. P.; Sentef, M. A.; Wolf, M.; Rubio, A.; et al. Ultrafast Dynamical Lifshitz Transition. *Sci. Adv.* **2021**, *7* (17), No. eabd9275.

(52) Guan, M.-X.; Wang, E.; You, P.-W.; Sun, J.-T.; Meng, S. Manipulating Weyl Quasiparticles by Orbital-Selective Photoexcitation in WTe_2 . *Nat. Commun.* **2021**, *12*, 1885.

(53) Xu, S.-Y.; Ma, Q.; Gao, Y.; Kogar, A.; Zong, A.; Mier Valdivia, A. M.; Dinh, T. H.; Huang, S.-M.; Singh, B.; Hsu, C.-H.; et al. Spontaneous Gyrotropic Electronic Order in a Transition-Metal Dichalcogenide. *Nature* **2020**, *578* (7796), 545–549.